Received: 17 June 2022 | Revised: 27 October 2022 | Accepted: 29 October 2022

IET Microwaves, Antennas & Propagation

DOI: 10.1049/mia2.12321

ORIGINAL RESEARCH

Ultra-thin electromagnetic bandgap backed fractal geometry-based antenna for 24 GHz ISM band WBAN

Mubasher Ali[1] | Irfan Ullah[2] | John C. Batchelor[1] | Nathan J. Gomes[1,3]

[1]School of Engineering, University of Kent, Canterbury, UK

[2]Department of Electronic and Computer Science, University of Southampton, Southampton, UK

[3]Department of Electronic and Electrical Engineering, UCL, London, UK

Correspondence

Mubasher Ali, School of Engineering, University of Kent, Room 1.18, Jennison building, Giles Ln, Canterbury, CT2 7NZ, UK.
Email: ma954@kent.ac.uk

Funding information

Engineering and Physical Sciences Research Council; UK Research and Innovation, Grant/Award Number: EP/S020160/1

Abstract

A compact, ultra-thin electromagnetic bandgap (EBG) backed antenna is presented for the 24 GHz ISM band for WBAN applications. The proposed antenna has Koch fractal geometry-based bow-tie slots, designed with an overall dimension of $0.91\lambda_0 \times 0.84\lambda_0 \times 0.01\lambda_0$ and backed by a 5×5 element $0.01\lambda_0$ thick EBG structure; it is fabricated on a flexible Rogers 5880 substrate (thickness = 0.127 mm and dielectric constant $\varepsilon_r = 2.2$, $\tan\delta = 0.0009$). In comparison to the previously published K band prototype antennas, our presented fractal antenna has a more compact and ultra-thin form factor. The low profile, via-less EBG unit cell structure with dimensions of $0.254\lambda_0 \times 0.254\lambda_0$, possesses both Artificial Magnetic Conductor (AMC) and EBG characteristics. It is straightforward to fabricate at a millimeter-scale. The performance parameters of the design are investigated in terms of on-body reflection coefficient and free-space radiation patterns with and without structural bending. The EBG structure enhances the antenna's front-lobe gain by 2.3 dB, decreases back-lobe radiation by 12.6 dB and decreases the specific absorption rate (SAR [1 g]) from >50.9 W/kg to <6.14 W/kg, significantly reducing the potential harm to the human body. Experimental investigations revealed high insensitivity of the proposed antenna to body proximity, and the performance is preserved with structural deformation.

1 | INTRODUCTION

Nowadays, wireless networks for wearables have gained substantial attention within both academic and industrial communities as they offer potential to further enhance the usage in military application, navigation, remote monitoring of healthcare systems and sporting performance [1, 2]. The millimeter-wave (mm-wave) spectrum offers many benefits such as large data rates, larger channel multiplexes, reduction in interference because of uncongested spectrum, miniaturisation of devices and unlicensed frequency bands [3]. Choosing 24 GHz (ISM) band over 60 GHz enables lower path-loss environment, less shadow fading and use of less directive antennas. However, wearable antennas for the body centric application have been mostly studied in the microwave spectrum rather than at mm-wave frequencies [4, 5]. Recently, two different inkjet-printed multilayer, multidirector mm-wave Yagi–Uda antennas have been developed on a thin flexible material for 24.5 GHz (ISM) band applications [6]. In Ref. [7], a wearable end-fire antenna has been proposed for 60 GHz on-body communication. However, these mm-wave body-worn antennas pose a potential radiation hazard to the human body because of high backward radiation (>5 dBi). The penetration depth of mm-waves to the human body is small due to the very short wavelength, and this restricts the risk to the skin. The value of the power transmission coefficient is extremely high in human tissues at mm-waves as compared to sub-6 GHz frequencies. Consequently, much of the electromagnetic energy is absorbed into the human skin. This issue can drastically decrease the efficiency of the antenna as well as cause a risk to the wearer's safety. Therefore, adequate isolation is necessary between the antenna and the human tissues [8]. An electromagnetic bandgap (EBG) structure is considered an effective approach to reduce harmful radiation by suppressing the back lobe and surface waves [9]. An EBG array in a phone case has been developed to minimise human exposure at microwave frequency in terms of SAR by 24%. This further reduces the effects of proximity of the human body and thereby enhances the gain of the antenna by 19% [10]. A textile-

based square EBG has been developed at 26 GHz that improved the gain by 2.52 dB [11].

In this study, an ultra-thin Koch fractal geometry-based antenna integrated with a compact EBG/AMC structure having a total thickness of $0.02\lambda_0$ is presented. The proposed antenna geometry consists of Koch fractal-based bow-tie slots on a radiating monopole, backed by a compact 5 × 5 cell EBG structure demonstrating both the bandgap and the required phase reflection at 24 GHz ISM band, which significantly reduces surface waves and the back-lobe of the antenna, respectively. The proposed structure uses extremely thin (127 μm) substrate of Rogers 5880 which made it flexible enough to fit on any shape or part of the human body. This structure is compact and electrically thinner than the comparable structures in literature. It also possesses a good bandwidth when attached directly to the skin, a minimum shift in S_{11} while bending, a comparable front-to-back ratio (FBR) with a 30% decrease in thickness and the largest decrease in SAR percentage when compared with the existing wearable EBG backed antennas in K band. The paper is organised as follows: Section 2 presents the design and characterisation of the Koch fractal bow-tie antenna structure and EBG/AMC structure. Section 3 presents the results of the prototyped EBG backed antenna in terms of the reflection coefficient S_{11}, radiations pattern, on-body operations, structural bending and SAR.

2 | EBG/AMC AND ANTENNA DESIGN

This section provides the geometry and structure of an EBG backed antenna. A split square ring resonator-based EBG geometry and Koch fractal bow-tie slot antenna are designed and investigated.

2.1 | EBG design

A unit cell of $W \times W = 3.18 \times 3.18$ mm^2 on a Rogers 5880 dielectric substrate ($\varepsilon_r = 2.2$) and thickness of 0.127 mm over a ground plane was simulated in CST Microwave Studio using periodic boundary conditions (PBCs), Figure 1a. The proposed EBG unit cell consists of an approximately one wavelength perimeter split square ring resonator with coupling gaps on two corners. The EBG structure is symmetric along both the X and Y-axis as shown in Figure 1a, and the equivalent LC behaviour acts as a two-dimensional electric filter within the 24 GHz ISM band, where the surface exhibits high impedance. The change in the dimension of trace width and coupling gap varies the operating region, that is, a decrease in the trace width and slot gap shifts the band gap region to lower frequencies. The unit cell was optimised to obtain the required phase reflection response at 24.125 GHz. This configuration provides 0° phase shift from the reflected wave and behaves as an artificial magnetic conductor (AMC). Figure 1b presents the simulated reflection phase diagram of a normally incident plane wave on the unit cell surface. The resonant frequency is 24.125 GHz, and the bandwidth is approximately 250 MHz. The AMC is a single layer and does not require vias, which simplifies the fabrication and reduces cost.

The characteristics of periodic EBG structures can be investigated by employing two different techniques such as the dispersion diagram and the suspended transmission line method. We analyse the bandgap region using both approaches. To calculate the dispersion diagram from the unit cell, periodic boundary conditions and an appropriate phase shift are applied to the sides. The unit cell repeats infinitely with periodicity P_x, P_y and lattice angle α. The CST Eigenmode Solver is used to generate the dispersion response in Figure 1c. The vertical axis shows frequency, while the horizontal represents transverse wavenumbers, specifically (Gamma), X and M as indicated in the inset. Hexahedral mesh type is used and the Jacobi–Davidson Method Eigenmode solver is chosen, which is considered to be faster for the given example. An EBG bandgap region from 23.9 to 24.48 GHz is observed, and surface waves will be suppressed in this band. Therefore, the interaction between the fields and the skin at the structure edge is reduced. The AMC characteristic improves the forward radiation, while the EBG effect improves the decoupling of the structure from the skin.

To further verify the bandgap region, the suspended transmission line approach was modelled using a 0.5 mm wide microstrip line placed on $0.02\lambda_0$ above a 5 × 5 EBG array. The simulated transmission coefficient is presented in Figure 2. The S_{21} is below −20 dB between 23.962 and 24.353 GHz.

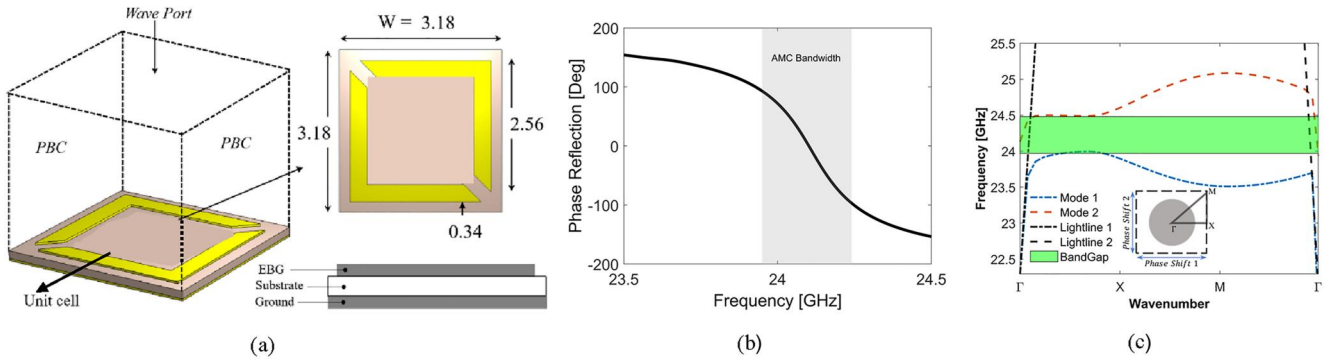

FIGURE 1 (a) Proposed EBG geometry, (b) phase reflection and (c) dispersion diagram.

2.2 | Antenna design and integration with EBG surface

In this subsection, the Koch fractal geometry-based slotted bow-tie antenna is presented in Figure 3a. To achieve flexibility, the antenna height is kept low, which reduces the impedance bandwidth. Then, the bandwidth of the proposed antenna is further enhanced by adding fractal repetition [12] along the resonant length of the patch. This fractal bow-tie slot antenna has single metallisation and dielectric layers, such that ungrounded coplanar waveguide feeding is a suitable option in terms of fabrication. After the integration of the antenna with the EBG array, grounded CPW feeding was chosen as the EBG array has a metal ground plane. The female type 50Ω SMA edge mount connector (HRM(G)-300-467B-1 specified to 28 GHz) was simulated with the full structure to improve the comparison with measurement. The fractal bow-tie slot antenna simulations were performed using the CST time domain solver, and a prototype was fabricated using chemical etching. A 5 × 5 EBG array was placed underneath the slot antenna. Figure 3b shows the dielectric and metal layer stack of the antenna-EBG structure. This prototype has an edge-mounted connector and no air gap between the layers. The EBG backed antenna was shown by measurement in Figure 3c to be well isolated from the skin, meaning the design process was valid without accounting for body loading. This configuration is suitable for wearing on the surface of the body. The resultant antenna is ultra-thin with overall dimensions of 16.19 × 16.19 × 0.254 mm^3.

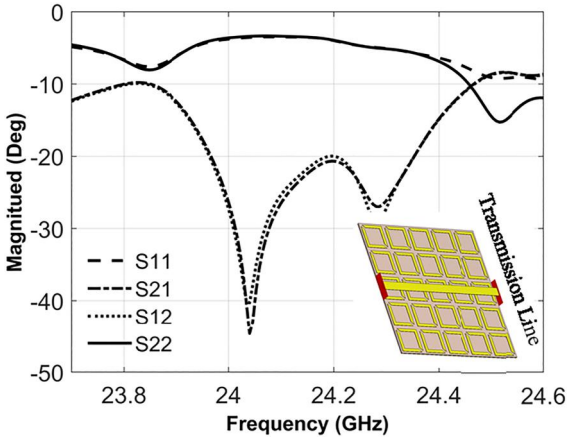

FIGURE 2 EBG suspended transmission line S parameters

3 | RESULTS AND DISCUSSIONS

This section presents the simulated and measured S_{11} and radiation patterns together with a consideration of body loading and a deformation study.

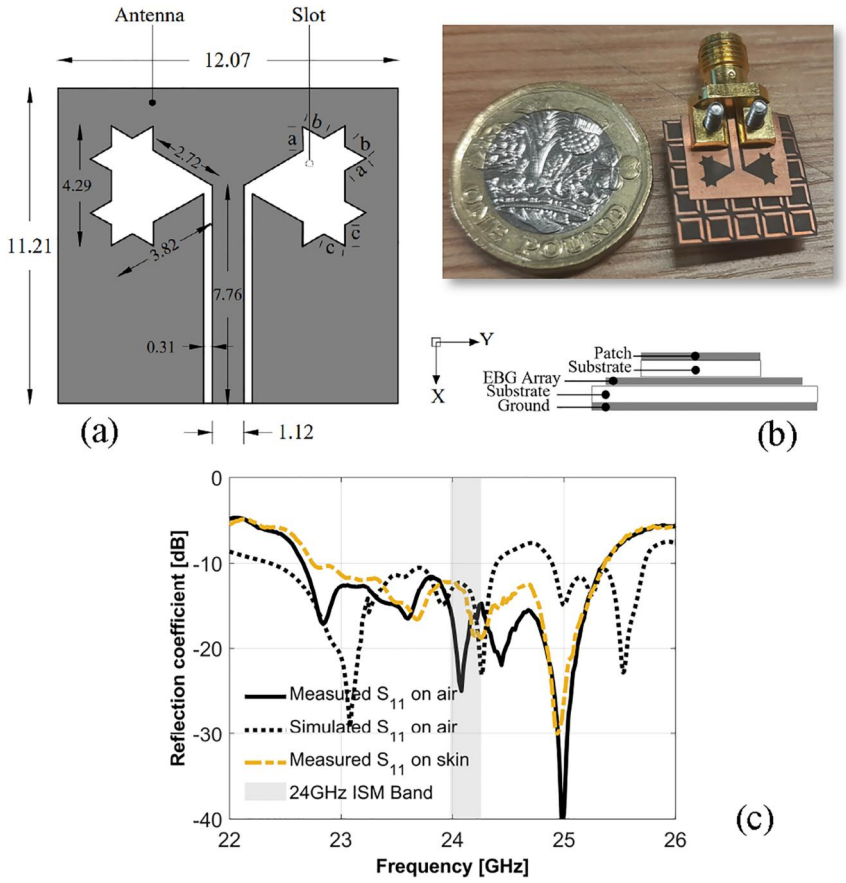

FIGURE 3 (a) The Koch fractal based bow-tie slot antenna geometry, $a = 0.72$, $b = 0.67$ and $c = 0.75$ mm (b) integration of EBG with antenna, (c) S_{11} of EBG backed antenna.

3.1 | Reflection coefficient evaluation

The prototype was tested in-house, and the measured reflection parameters taken with a 65 GHz VNA (Anritsu 37397c). Figure 3c shows that the S_{11} values are less than −10 dB from 22.6 GHz to 25. 35 GHz (bandwidth of 2.75 GHz). The shaded bar in Figure 3c shows that the simulated and measured reflection coefficient of the EBG-backed antenna is below −15 dB in the ISM band (24–24.250 GHz). This investigation considers the antenna for the application in the 24 GHz ISM band. So although the structure is a wider band, this additional performance is not required here.

3.2 | Far-field radiation properties

The far-field radiation measurements were taken in an anechoic chamber. Figure 4 shows the H- and E-plane polar plots with and without the EBG/AMC array structure at 24 GHz. Placing the EBG/AMC structure underneath the antenna suppresses the back lobe by 12.6 dB at 24 GHz, whereas the realised gain increases by 2.3 dB to 5.1 dBi at 24 GHz. The results indicate the effectiveness of the EBG/AMC structure in suppressing surface waves and reflecting radiation away from the human body.

Simulated radiation patterns on and off skin are included in Figure 4. It can be seen that the EBG reduces the skin loading effect, such that the difference at a given angle in the rear hemisphere is within about 10 dB.

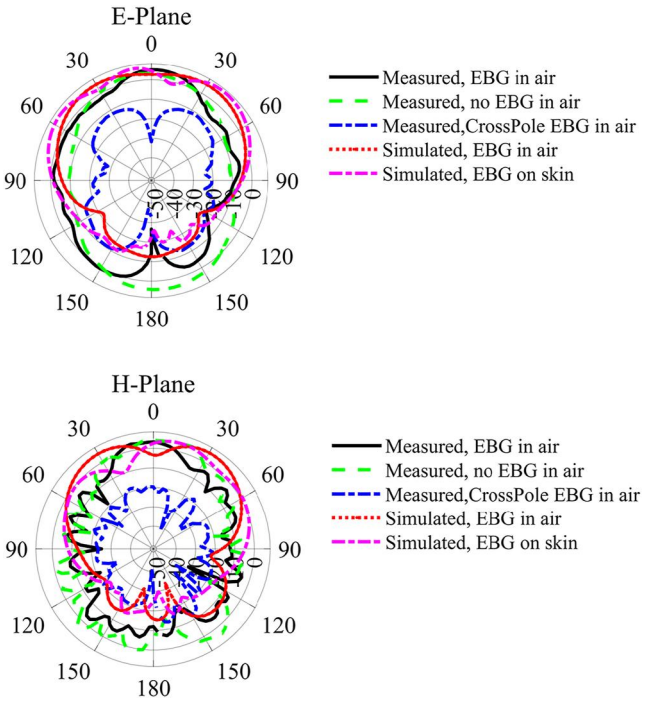

FIGURE 4 Measured and simulated radiation polar plots of EBG backed antenna

3.3 | On-body performance

As the proposed EBG suppresses backward radiation, the prototype antenna should be tolerant to human tissue loading. On-body measurements were performed on the chest, forehead, thigh and wrist of a male volunteer who weighed 61 kg and was 178 cm in height. The S_{11} of the human body loaded antenna is presented in Figure 5a. The curves differ due to the varying capacitive and dielectric constant values of human tissues at different mounting sites. However, apart from the thigh, all the measured S_{11} were at <−10 dB over the desired 24 GHz ISM band. Figure 5a illustrates that without an EBG/AMC, the structure is highly lossy across the entire measured band, and the antenna is detuned in all cases. When the EBG/AMC is added, Figure 5b, the structure is tuned for the ISM band for all mounting sites, and the out-of-band loss decreases by around 5 dB. The prototype not only covers the 24 GHz ISM band but has 2.7 GHz bandwidth. Hence, this optimised EBG-backed Koch fractal bow-tie slot antenna with stable S_{11} response when attached to the body is a suitable candidate for 24 GHz ISM band wearable applications.

3.4 | Structural conformability

The chosen antenna placement positions in Figure 5 can be considered as relatively flat. However, the capability to bear some structural deformation while retaining radiation performance with close conformance to the curved surface of the

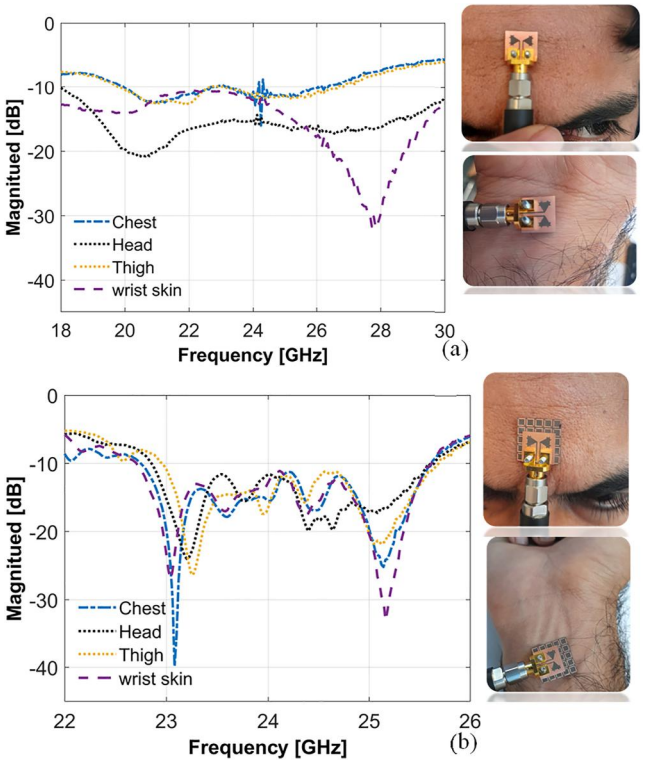

FIGURE 5 Measured reflection coefficients of the antenna on the human body (a) without EBG (b) with EBG.

body is important for on-skin mounting. Therefore, the structure was further investigated under bending conditions. Figure 6 shows the reflection coefficient measurements when the antenna is bent around a polyethylene foam cylinder separately along the X and the Y-axis. The dielectric constant of the available polyethylene is between 1.3 and 1.6. A tissue phantom was not used, as it has been shown that the antenna is not strongly loaded by the body and therefore the curvature effect would dominate. Due to the reduction in the resonant length while bending, a slight shift in centre frequency can be seen from the plot when bent along the X-axis. A severe detuning and a shift of 400 MHz is observed when bent along the Y-axis. However, even with a 14 mm radius of curvature, the EBG backed bow-tie slot antenna still achieves reasonable reflection coefficient values (<-10 dB) at 24 GHz ISM band.

Furthermore, Figure 7 presents the radiation patterns under bending for radii R_x and $R_y = 14$ mm along the Y- and X-axis. The directivity is seen to be around -2.1 dB for both axes of curvature.

3.5 | Specific absorption rate (SAR) evaluation

To investigate the performance of the antenna in terms of the specific absorption rate (SAR), a rectangular block three-layer skin-fat-muscle model (Figure 8c) is used in CST MWS. Table 1 presents the dielectric properties of dry skin, fat and muscle layers, which were obtained from the online website of the Italian National Research Council [13]. The total size of the three-layer tissue model was $50 \times 30 \times 6$ mm^3. For the SAR evaluation there was a 2 mm gap between the skin and the EBG ground plane due to the height of the connector. Figure 8 presents the SAR distribution using the IEEE/IEC 62704-1 averaging technique for 1 g of tissue volume. The maximum SAR values were 6.14 and 50.93 W/kg at 200 mW input power, respectively. Thus, in the EBG case, the maximum SAR was reduced by 90% compared to the direct exposure from the antenna. To further analyse the effectiveness of the EBG structure, the rear ground plane without an EBG element array is placed underneath the antenna. The proposed antenna becomes 3.57 mm thick to get the required reflection coefficient performance at 24 GHz, and a significant decrease in the front-to-back ratio has also been observed. Therefore, the proposed EBG element is responsible for the ultra-thin structure of the antenna.

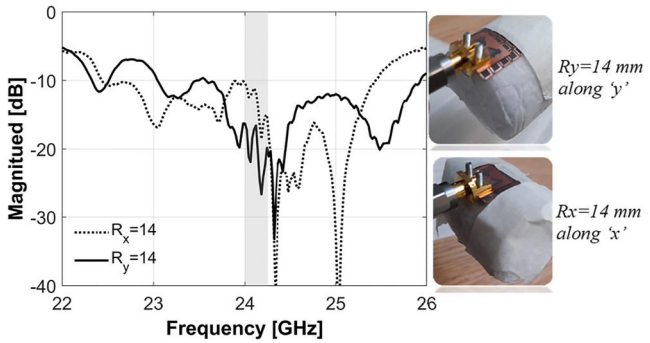

FIGURE 6 reflection coefficient of the electromagnetic bandgap (EBG) backed antenna when bent along 'Y' and 'X'

4 | CONCLUSION

In this study, a novel, ultra-thin and compact EBG-backed Koch fractal antenna structure is presented. Its periodic structure shows both AMC and EBG characteristics in the 24 GHz ISM band. The 5×5 element EBG array is evaluated beneath a Koch fractal bow-tie slot antenna and to the authors' knowledge is the thinnest ($0.02\lambda_0$) EBG-backed antenna reported in the K band. Table 2 presents the comparisons of different features of the proposed antenna with previously published K band EBG integrated antennas. The proposed antenna is the thinnest and smallest in size. This antenna also possesses a large bandwidth of 11.25% when attached directly to the skin; a minimum shift in S_{11} while bending, a high increase in FBR and the largest decrease in SAR percentage. Anechoic chamber measurements of the EBG-backed antenna show a significant improvement in gain by 2.3 dB and in the FBR by 14.9 dB. The reflection coefficient performance of the antenna with EBG while attached to the human skin shows good insensitivity to body proximity.

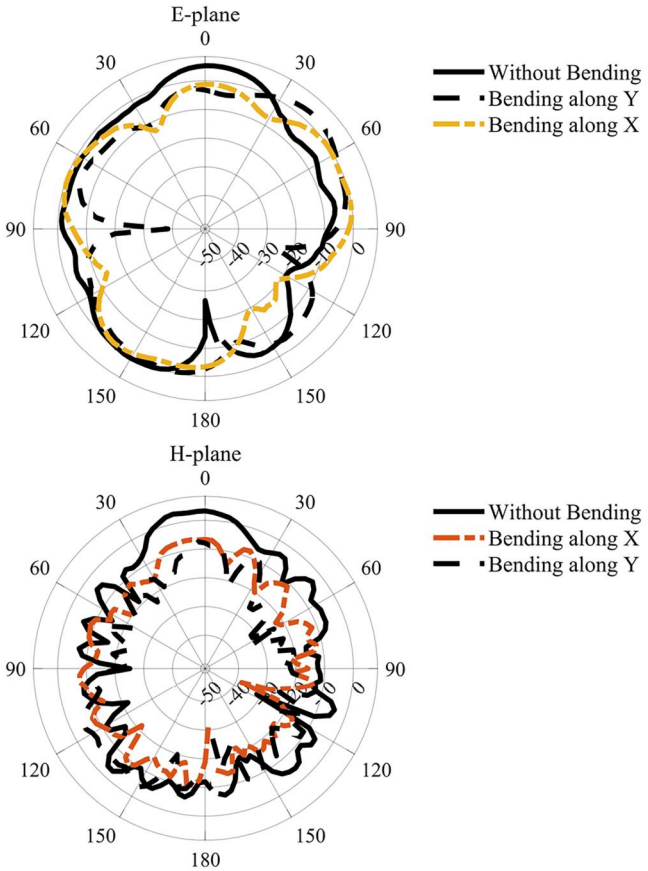

FIGURE 7 Measured radiation polar plots of EBG backed antenna when bent on 14 mm radius cylinder along the X-axis (Red dash-line), Y-axis (orange dash-line) and without bending (solid-line) at 24 GHz.

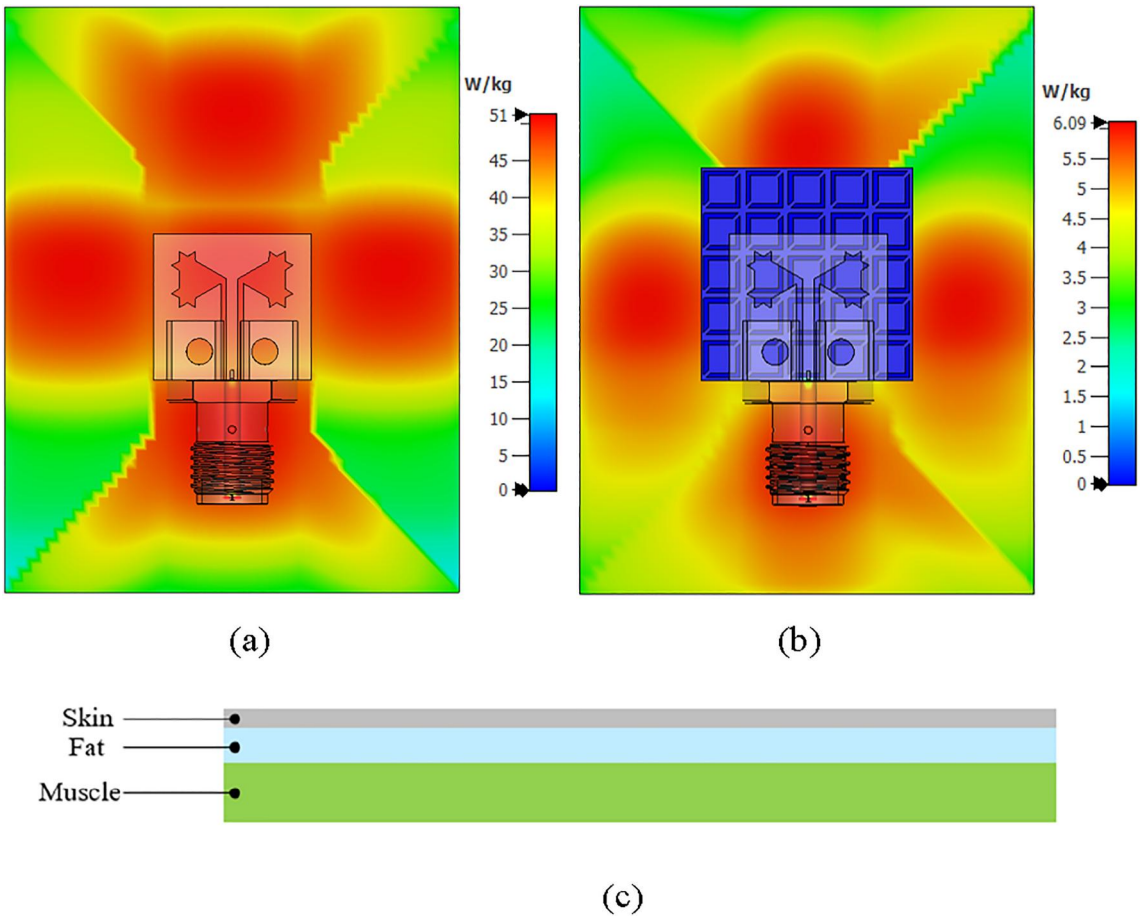

FIGURE 8 SAR distribution of prototype antenna (a) without EBG (b) with EBG (c) placement setting of tissues. Note, different scales are used in (b) and (c) owing to large variation in peak values. EBG, electromagnetic bandgap.

TABLE 1 Material properties of skin, fat and muscle tissues at 24 GHz

Material	Dielectric constant ε_r	Loss tangent tanδ	Penetration depth (mm)	Conductivity (S/m)	Thickness (mm)
Skin	18.99	0.90073	1.097	22.841	1.5
Fat	3.84	0.29076	7.053	1.489	2
Muscle	27.39	0.80483	1.008	29.437	2.5

TABLE 2 Comparison of the proposed antenna with previously reported K band electromagnetic bandgap (EBG) antennas

Ref	Freq. GHz	Dimension λ_0	Thickness λ_0	Gain dBi	Antenna-body gap	On-body S_{11} BW(GHz/%)	S_{11} shift MHz/radii mm	Gain/bending radius mm	Increase in FBR	Decrement in SAR
Proposed	24	1.29 × 1.29	0.02	5.08	On skin	2.7/11.3%	400/14	−2.1 dBi/14	14.9 dB	90%
[14]	26	2.79 × 1.91	0.03	8.65	On skin	0.6/2.3%	~400/30	N\A	2 dB	69.9%
[11]	28	2.67 × 3.14	0.07	7.90	Adhesive + Fabric	10/40%	~1500/30	N\A	15 dB	N\A
[15]	24	2.16 × 2.16	0.05	6	Fabric	~0.7/3%	~400/30	5.3 dBi/30[a]	9.9 dB	N\A
[16]	28	1.90 × 1.90	0.14	5.20	N\A	0.9/3.3%[b]	N\A	N\A	N\A	N\A

[a]Simulated gain when bent along 30 mm radius cylinder.

[b]Free space impedance bandwidth.

Furthermore, EBG-backed antenna structural deformation performed over a curve of 14 mm radius results in only slight detuning of the centre frequency and insignificant variation in bandwidth. The radiation pattern of the curved EBG antenna shows reasonable directivity and a gain of −2.1 dB under bending. Finally, the SAR simulation of the antenna over a three-layer skin-fat-muscle model under standard 200 mW input power shows a 90% reduction in SAR due to the EBG screen, which demonstrates suitability for 24 GHz ISM band conformally mounted WBAN applications.

AUTHOR CONTRIBUTIONS

Mubasher Ali: Conceptualisation; Formal analysis; Investigation; Methodology; Software; Visualisation; Writing—original draft. **Irfan Ullah:** Data curation. **John C. Batchelor:** Resources; Supervision; Investigation; Validation; Writing–review & editing. **Nathan J. Gomes:** Supervision; Writing—review & editing.

ACKNOWLEDGEMENTS

This work was supported by the Engineering and Physical Sciences Research Council (ESPRC) operating under UK Research and Innovation (UKRI) under grant no. EP/S020160/1.

CONFLICT OF INTEREST

The authors have no conflicts of interest to declare. All co-authors have seen and agree with the contents of the manuscript.

DATA AVAILABILITY STATEMENT

The data that support the findings of this study are available from the corresponding author upon reasonable request.

ORCID

Mubasher Ali https://orcid.org/0000-0003-0978-8239

REFERENCES

1. Aun, N.F.M., et al.: Revolutionizing wearables for 5G: 5G technologies: recent developments and future perspectives for wearable devices and antennas. IEEE Microw. Mag. 18(3), 108–124 (2017). https://doi.org/10.1109/MMM.2017.2664019
2. Ali, M., et al.: Multiband ultra-thin flexible on-body transceivers for wearable health informatics. Australas. Phys. Eng. Sci. Med. 42(1), 53–63 (2019). https://doi.org/10.1007/s13246-018-0711-2
3. Attia, H., Abdelghani, M.L., Denidni, T.A.: Wideband and high-gain millimeter-wave antenna based on FSS Fabry–Perot cavity. IEEE Trans antennas propagation. 65(10), 5589–5594 (2017). https://doi.org/10.1109/TAP.2017.2742550
4. Ukkonen, L., Sydänheimo, L., Rahmat-Samii, Y.: Embroidered textile antennas for wireless body-centric communication Cand sensing. In: 2015 Loughborough Antennas & Propagation Conference (LAPC). IEEE (2015). https://doi.org/10.1109/LAPC.2015.7366011
5. Arif, A., et al.: A compact, low-profile fractal antenna for wearable on-body WBAN applications. IEEE Antenn. Wireless Propag. Lett. 18(5), 981–985 (2019). https://doi.org/10.1109/LAWP.2019.2906829
6. Tehrani, B.K., Cook, B.S., Tentzeris, M.M.: Inkjet printing of multilayer millimeter-wave Yagi-Uda antennas on flexible substrates. IEEE Antenn. Wireless Propag. Lett. 15, 143–146 (2015). https://doi.org/10.1109/LAWP.2015.2434823
7. Chahat, N., et al.: Wearable endfire textile antenna for on-body communications at 60 GHz. IEEE Antenn. Wireless Propag. Lett. 11, 799–802 (2012). https://doi.org/10.1109/LAWP.2012.2207698
8. Wang, M., et al.: Investigation of SAR reduction using flexible antenna with metamaterial structure in wireless body area network. IEEE Trans. Antenn. Propag. 66(6), 3076–3086 (2018). https://doi.org/10.1109/TAP.2018.2820733
9. Wu, T., et al.: The human body and millimeter-wave wireless communication systems: interactions and implications. In: 2015 IEEE International Conference on Communications (ICC), pp. 2423–2429. (2015). https://doi.org/10.1109/icc.2015.7248688
10. Das, R., Yoo, H.: Application of a compact electromagnetic bandgap array in a phone case for suppression of mobile phone radiation exposure. IEEE Trans. Microw. Theor. Tech. 66(5), 2363–2372 (2018). https://doi.org/10.1109/TMTT.2017.2786287
11. Lin, X., et al.: Flexible fractal electromagnetic bandgap for millimeter-wave wearable antennas. IEEE Antenn. Wireless Propag. Lett. 17(7), 1281–1285 (2018). https://doi.org/10.1109/LAWP.2018.2842109
12. Soliman, E.A., et al.: Bow-tie slot antenna fed by CPW. Electron. Lett. 35(7), 514–515 (1999). https://doi.org/10.1049/el:19990399
13. Andreuccetti, D., et al.: An Internet Resource for the Calculation of the Dielectric Properties of Body Tissues in the Frequency Range 10 Hz-100 GHz (2012). http://niremf.ifac.cnr.it/tissprop/
14. Wissem, E.L.M., et al.: A textile EBG-based antenna for future 5G-IoT millimeter-wave applications. Electronics 10(2), 154 (2021). https://doi.org/10.3390/electronics10020154
15. Iqbal, A., et al.: Electromagnetic bandgap backed millimeter-wave MIMO antenna for wearable applications. IEEE Access 7, 111135–111144 (2019). https://doi.org/10.1109/ACCESS.2019.2933913
16. Ashraf, N., et al.: 28/38-GHz dual-band millimeter wave SIW array antenna with EBG structures for 5G applications. In: International Conference on Information and Communication Technology Research (ICTRC). IEEE (2015). https://doi.org/10.1109/ICTRC.2015.7156407

SUPPORTING INFORMATION

Additional supporting information can be found online in the Supporting Information section at the end of this article.

How to cite this article: Ali, M., et al.: Ultra-thin electromagnetic bandgap backed fractal geometry-based antenna for 24 GHz ISM band WBAN. IET Microw. Antennas Propag. 17(3), 216–222 (2023). https://doi.org/10.1049/mia2.12321